Annals of Nuclear Energy 116 (2018) 152–162

Contents lists available at ScienceDirect

Annals of Nuclear Energy

journal homepage: www.elsevier.com/locate/anucene

Investigation of flow instability using axially decreased power shape in parallel channels with water at supercritical pressure

Edward Shitsi *, Seth Kofi Debrah, Vincent Yao Agbodemegbe, Emmanuel Ampomah-Amoako

Department of Nuclear Engineering, School of Nuclear and Allied Sciences, University of Ghana, P.O. Box AE 1, Atomic Energy, Kwabenya, Accra, Ghana

ARTICLE INFO

Article history:
Received 20 February 2017
Received in revised form 7 January 2018
Accepted 19 February 2018

Keywords:
Numerical study
Supercritical pressure
Flow instability
Axially decreased power shape
Parallel channels

ABSTRACT

Realizing the economic viability of SCWR, a GEN IV reactor, several research activities have been carried to address challenges associated with a system operated at supercritical pressures as a result of drastic changes in fluid properties at these supercritical pressures. These challenges include enhanced heat transfer EHT, deteriorated heat transfer HTD and flow instability among many others. The research activities mostly focused on CFD and experimental studies involving single tube due to the complexity of parallel channel flow and other non-circular flow geometries. Research in parallel channels is needed to address related supercritical heat transfer challenges and to provide more realistic information to the SCWR core design.

This study investigated flow instability in parallel channels with water at supercritical pressures adopting axially decreased power shape ADPS. The effects of pressure, mass flow rate, and gravity on flow instability were investigated. Sensitivity analysis of some selected turbulence models and time steps were first carried out with the aim of selecting suitable turbulence model and time step for the numerical simulations. For the system operated at system pressure of 23 MPa, inlet temperatures from 180 °C to 360 °C, and system mass flow rates of 125 kg/h and 145 kg/h, the system stability decreases with inlet temperature at the high mass flow rate with only lower threshold as instability boundary, but there is a threshold power corresponding to a particular inlet temperature below which stability decreases and above which stability increases with inlet temperature for the low mass flow rate. The system stability increases with increase of system mass flow rate at low inlet temperatures, but decreases with increase of system mass flow rate at high inlet temperatures. With the increase of system pressure at 125 kg/h to 25 MPa, there is different threshold power with particular inlet temperature below which stability decreases and above which stability increases with inlet temperature. The system operated at high pressure is more stable than that operated at low pressure. The effect of stability of a system operated with or without gravity influence is similar to that of the system operated at low pressure or at high pressure respectively. The system operated without gravity influence is more stable than that operated with gravity influence. For the system operated at system pressure of 23 MPa, inlet temperatures from 180 °C to 260 °C, and system mass flow rates of 125 kg/h and 145 kg/h, the trends of the numerical results are in agreement with the trends of the experimental results. The obtained numerical instability boundary finding that the system is more stable at larger mass flow rate is the opposite of the corresponding experimental instability boundary finding. The numerical dynamics characteristics finding that the system is more stable at low mass flow rate contradicts the corresponding experimental dynamics characteristics finding that mass flow rate has less effect on flow instability. The numerical tool predicted quite close to the experimental results at larger mass flow rate. The numerical tool adopted largely under-predicted experimental amplitude and quite well predicted experimental period of the inlet mass flow oscillations. The adopted 3D numerical tool, STAR-CCM+ code could capture dynamics characteristics of the flow quite well and also predict flow instability in the parallel channels. However, there is evidence that the presence of heating structures in the geometrical model adopted may change the predicted behavior, as shown in previous works. More relevant experiments at supercritical pressures should be carried out for validation of numerical tools adopted for similar studies.

* Corresponding author.
E-mail addresses: edwardshitsi@yahoo.com (E. Shitsi), s.debrah@gaecgh.org (S.K. Debrah).

https://doi.org/10.1016/j.anucene.2018.02.035
0306-4549/

Nomenclature

$C_{1\varepsilon}, C_{2\varepsilon}, C_{3\varepsilon}$	turbulence model coefficients
D_H	hydraulic diameter (m)
g	acceleration due gravity (m/s^2)
G	mass flux (kg/m^2 s)
D_w	cross diffusion term (kg/m s^4)
G_b	generation of turbulence kinetic energy due to buoyancy (kg J/m^3 s)
G_k	generation of turbulence kinetic energy due to mean velocity gradient (kg J/m^3 s)
G_ω	generation of ω (kg/m s^4)
K	hydraulic loss coefficient
K_{in}	localized pressure drop coefficient at the channel inlet
K_{out}	localized pressure drop coefficient at the channel outlet
L	length of the pipe (m)
L_H	heated length (m)
M_t	total mass flow rate (kg/s)
p	system pressure (Pa)
Re	Reynolds number ($Re = GD/\mu$)
S_k	source term in k equation (kg J/m^3 s)
S_T	source term in energy equation (kg K/m^3 s)
S_u	source term in x momentum equation (kg/m^2 s^2)
S_v	source term in y momentum equation (kg/m^2 s^2)
S_w	source term in z momentum equation (kg/m^2 s^2)
S_ε	source term in ε equation (kg/m s^4)
S_ω	source term in ω equation (kg/m s^4)
T	temperature (K)
u	velocity (m/s)

Greek letters

ε	turbulent dissipation rate (m^2/s^3)
ω	specific turbulent dissipation rate (1/s)
λ	thermal conductivity (W/m K)
k	turbulent kinetic energy, m^2/s^2
μ	viscosity (Pas)
μ_t	turbulent viscosity (Pas)
ρ	density of the fluid (kg/m^3)
σ_k	Prandtl number ($Pr = \mu C_p/\lambda$) correspond to k
σ_ε	Prandtl number ($Pr = \mu C_p/\lambda$) correspond to ε
σ_ω	Prandtl number ($Pr = \mu C_p/\lambda$) correspond to ω
τ_k	Effective diffusivity of k (kg/m s)
τ_ω	Effective diffusivity of ω (kg/m s)

Subscripts

b	bulk
g	gravity
in	inlet
out	outlet
p	constant pressure
pc	pseudo-critical

Abbreviations

ADPS	Axially Decreased Power Shape/distribution
GEN	Generation
NPIC	Nuclear Power Institute of China
SCWR	Supercritical Water-cooled Reactor

1. Introduction

Realizing the economic viability of SCWR, a GEN IV reactor, several research activities have been carried to address challenges associated with a system operated at supercritical pressures as a result of drastic changes in fluid properties at these supercritical pressures (Figs. 1–4) (Ambrosini, 2007; Ambrosini and Sharabi, 2007, 2008; Chatoorgoon, 2001, 2006; Xi et al., 2014a,b). These challenges include enhanced heat transfer EHT, deteriorated heat transfer HTD and flow instability among many others. These research activities would also broaden the existing knowledge on flow instability at supercritical pressures in different flow geometries. Fig. 5 shows typical flow oscillations of mass flow rate obtained at the inlet of the heated channels. The flow oscillations start to develop as a result of continuous heat application to the heated parallel channels. The system flow is stable up to 7 s. Flow oscillations start to develop beyond 7 s. At this point, the system conditions develop up to the conditions near the vicinity of critical and pseudo-critical points where the fluid properties (density, specific heat, viscosity and thermal conductivity) start to develop sharp variations (Figs. 1–4). Beyond the vicinity of critical and pseudo-critical points, the fluid properties show less variations similar to variations obtained before the vicinity of critical and pseudo-critical points (Figs. 1–4).

Ambrosini (2011), Ampomah-Amoako and Ambrosini (2013), Ampomah-Amoako (2013) reported that a basic continuity between the static Ledinegg instability and the dynamic density-

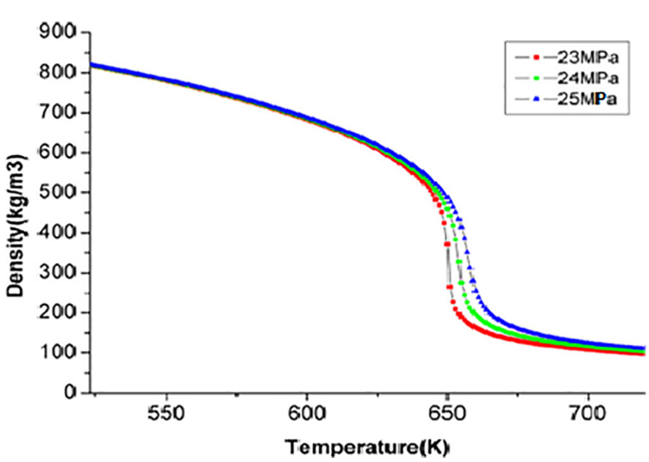

Fig. 1. Density change of water with the increase of temperature.

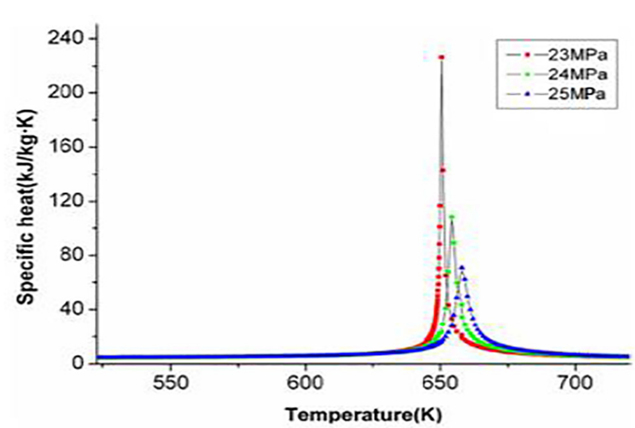

Fig. 2. Specific heat change of water with the increase of temperature.